Article:
Adlarson, P., Afzal, F., Aguar-Bartolomé, P. et al. (47 more authors) (2017) Measurement of the π0→e+e-γ Dalitz decay at the Mainz Microtron. Physical Review C. 025202. ISSN 2469-9993

https://doi.org/10.1103/PhysRevC.95.025202

Measurement of the $\pi^0 \to e^+e^-\gamma$ Dalitz decay at the Mainz Microtron

P. Adlarson,[1] F. Afzal,[2] P. Aguar-Bartolomé,[1] Z. Ahmed,[3] C. S. Akondi,[4] J. R. M. Annand,[5] H. J. Arends,[1] K. Bantawa,[4] R. Beck,[2] H. Berghäuser,[6] M. Biroth,[1] N. S. Borisov,[7] A. Braghieri,[8] W. J. Briscoe,[9] S. Cherepnya,[10] F. Cividini,[1] C. Collicott,[11,12] S. Costanza,[8,13] A. Denig,[1] M. Dieterle,[14] E. J. Downie,[1,9] P. Drexler,[1] M. I. Ferretti Bondy,[1] L. V. Fil'kov,[10] S. Gardner,[5] S. Garni,[14] D. I. Glazier,[5,15] D. Glowa,[15] W. Gradl,[1] G. M. Gurevich,[16] D. J. Hamilton,[5] D. Hornidge,[17] G. M. Huber,[3] T. C. Jude,[15] A. Käser,[14] V. L. Kashevarov,[1,10] S. Kay,[15] I. Keshelashvili,[14] R. Kondratiev,[16] M. Korolija,[18] B. Krusche,[14] V. V. Kulikov,[19] A. Lazarev,[7] J. Linturi,[1] V. Lisin,[10] K. Livingston,[5] I. J. D. MacGregor,[5] R. Macrae,[5] D. M. Manley,[4] P. P. Martel,[1,20] M. Martemianov,[19] J. C. McGeorge,[5] E. F. McNicoll,[5] V. Metag,[6] D. G. Middleton,[1,17] R. Miskimen,[20] E. Mornacchi,[1] C. Mullen,[5] A. Mushkarenkov,[8,20] A. Neganov,[7] A. Neiser,[1] A. Nikolaev,[2] M. Oberle,[14] M. Ostrick,[1] P. Ott,[1] P. B. Otte,[1] D. Paudyal,[3] P. Pedroni,[8] A. Polonski,[16] S. Prakhov,[1,21,*] A. Rajabi,[20] J. Robinson,[5] G. Ron,[22] G. Rosner,[5] T. Rostomyan,[14] C. Sfienti,[1] M. H. Sikora,[15] V. Sokhoyan,[1,9] K. Spieker,[2] O. Steffen,[1] I. I. Strakovsky,[9] B. Strandberg,[5] Th. Strub,[14] I. Supek,[18] A. Thiel,[2] M. Thiel,[1] A. Thomas,[1] M. Unverzagt,[1] Yu. A. Usov,[7] S. Wagner,[1] N. Walford,[14] D. P. Watts,[15] D. Werthmüller,[5,14] J. Wettig,[1] L. Witthauer,[14] M. Wolfes,[1] and L. A. Zana[15]

(A2 Collaboration at MAMI)

[1]*Institut für Kernphysik, University of Mainz, D-55099 Mainz, Germany*
[2]*Helmholtz-Institut für Strahlen- und Kernphysik, University of Bonn, D-53115 Bonn, Germany*
[3]*University of Regina, Regina, Saskatchewan S4S 0A2, Canada*
[4]*Kent State University, Kent, Ohio 44242-0001, USA*
[5]*SUPA School of Physics and Astronomy, University of Glasgow, Glasgow G12 8QQ, United Kingdom*
[6]*II Physikalisches Institut, University of Giessen, D-3539 Giessen, Germany*
[7]*Joint Institute for Nuclear Research, 141980 Dubna, Russia*
[8]*INFN Sezione di Pavia, I-27100 Pavia, Italy*
[9]*The George Washington University, Washington, DC 20052-0001, USA*
[10]*Lebedev Physical Institute, 119991 Moscow, Russia*
[11]*Dalhousie University, Halifax, Nova Scotia B3H 4R2, Canada*
[12]*Saint Marys University, Halifax, Nova Scotia B3H 3C3, Canada*
[13]*Dipartimento di Fisica, Università di Pavia, I-27100 Pavia, Italy*
[14]*Institut für Physik, University of Basel, CH-4056 Basel, Switzerland*
[15]*School of Physics, University of Edinburgh, Edinburgh EH9 3JZ, United Kingdom*
[16]*Institute for Nuclear Research, 125047 Moscow, Russia*
[17]*Mount Allison University, Sackville, New Brunswick E4L 1E6, Canada*
[18]*Rudjer Boskovic Institute, HR-10000 Zagreb, Croatia*
[19]*Institute for Theoretical and Experimental Physics, SRC Kurchatov Institute, Moscow 117218, Russia*
[20]*University of Massachusetts, Amherst, Massachusetts 01003, USA*
[21]*University of California Los Angeles, Los Angeles, California 90095-1547, USA*
[22]*Racah Institute of Physics, Hebrew University of Jerusalem, Jerusalem 91904, Israel*

(Received 16 November 2016; published 9 February 2017)

The Dalitz decay $\pi^0 \to e^+e^-\gamma$ has been measured in the $\gamma p \to \pi^0 p$ reaction with the A2 tagged-photon facility at the Mainz Microtron, MAMI. The value obtained for the slope parameter of the π^0 electromagnetic transition form factor, $a_\pi = 0.030 \pm 0.010_{\text{tot}}$, is in agreement with existing measurements of this decay and with recent theoretical calculations. The uncertainty obtained in the value of a_π is lower than in previous results based on the $\pi^0 \to e^+e^-\gamma$ decay.

DOI: 10.1103/PhysRevC.95.025202

I. INTRODUCTION

The electromagnetic (e/m) transition form factors (TFFs) of light mesons play an important role in understanding the properties of these particles as well as in low-energy precision tests of the standard model (SM) and quantum chromodynamics (QCD) [1]. These TFFs appear as input information for data-driven approximations and model calculations, including such quantities as rare pseudoscalar decays [2,3]. In particular, the TFFs of light mesons enter as contributions to the hadronic light-by-light (HLbL) scattering calculations [4,5] that are important for more accurate theoretical determinations of the anomalous magnetic moment of the muon, $(g-2)_\mu$, within the SM [6,7]. Recently, data-driven approaches, using dispersion relations, have been proposed [4,5,8] to attempt a better determination of the HLbL contribution to $(g-2)_\mu$ in a model-independent way. The precision of the calculations used to describe the HLbL contributions to $(g-2)_\mu$ can then be tested by directly comparing theoretical predictions from these

*Corresponding author: prakhov@ucla.edu

approaches for e/m TFFs of light mesons with experimental data.

The TFF parameters that can be extracted from the Dalitz decay of the lightest meson, $\pi^0 \to e^+e^-\gamma$, are important to constrain calculations that estimate the pion-exchange term, $a_\mu^{\pi^0}$, to the HLbL scattering contribution to $(g-2)_\mu$ [6]. The precise knowledge of the π^0 TFF is essential for a precision calculation of the decay width of the rare decay $\pi^0 \to e^+e^-$, the experimental value of which is in some disagreement with SM predictions [2,3]. In addition, this Dalitz decay recently attracted special attention because of a search for a hypothetical dark photon, γ', that could be looked for here via the decay chain $\pi^0 \to \gamma'\gamma \to e^+e^-\gamma$ [9–11].

For a structureless (pointlike) meson A, its decays into a lepton pair plus a photon, $A \to l^+l^-\gamma$, can be described within quantum electrodynamics (QED) via $A \to \gamma^*\gamma$, with the virtual photon γ^* decaying into the lepton pair [12]. For the meson A, QED predicts a specific strong dependence of its decay rate on the dilepton invariant mass, $m_{ll} = q$. A deviation from the pure QED dependence, caused by the actual electromagnetic structure of the meson A, is formally described by its e/m TFF [13]. The vector-meson-dominance (VMD) model [14] can be used to describe the coupling of the virtual photon γ^* to the meson A via an intermediate virtual vector meson V. This mechanism is especially strong in the timelike (the energy transfer larger than the momentum transfer) momentum-transfer region, $(2m_l)^2 < q^2 < m_A^2$, where a resonant behavior near $q^2 = m_V^2$ of the virtual photon arises because the virtual vector meson is approaching the mass shell [13], or even reaching it, as it is in the case of the $\eta' \to l^+l^-\gamma$ decay. Experimentally, timelike TFFs can be determined by measuring the actual decay rate of $A \to l^+l^-\gamma$ as a function of the dilepton invariant mass $m_{ll} = q$, normalizing this dependence to the partial decay width $\Gamma(A \to \gamma\gamma)$, and then taking the ratio to the pure QED dependence for the decay rate of $A \to \gamma^*\gamma \to l^+l^-\gamma$.

Because of the smallness of the π^0 mass, the virtual photon γ^* in the Dalitz decay of π^0 can produce only the lightest lepton pair, e^+e^-, with $m_{ee} = q$. Based on QED, the decay rate of $\pi^0 \to \gamma^*\gamma \to e^+e^-\gamma$ can be parametrized as [13]

$$\frac{d\Gamma(\pi^0 \to e^+e^-\gamma)}{dm_{ee}\Gamma(\pi^0 \to \gamma\gamma)} = \frac{4\alpha}{3\pi m_{ee}}\left(1-\frac{4m_e^2}{m_{ee}^2}\right)^{\frac{1}{2}}\left(1+\frac{2m_e^2}{m_{ee}^2}\right) \times \left(1-\frac{m_{ee}^2}{m_{\pi^0}^2}\right)^3 |F_{\pi^0\gamma}(m_{ee})|^2 = [\mathrm{QED}(m_{ee})]|F_{\pi^0\gamma}(m_{ee})|^2, \quad (1)$$

where $F_{\pi^0\gamma}$ is the normalized TFF of the π^0 meson, m_{π^0} and m_e are the masses of the π^0 meson and $e^{+/-}$, respectively. Because of the smallness of the momentum-transfer range for the $\pi^0 \to e^+e^-\gamma$ decay, its normalized TFF is typically parametrized as [15]

$$F_{\pi^0\gamma}(m_{ee}) = 1 + a_\pi \frac{m_{ee}^2}{m_{\pi^0}^2}, \quad (2)$$

where the parameter a_π reflects the TFF slope at $m_{ee} = 0$. A simple VMD model incorporates only the ρ, ω, and ϕ resonances (in the narrow-width approximation) as virtual vector mesons driving the photon interaction in $A \to \gamma^*\gamma$. Using a quark model for the corresponding couplings leads to neglecting ϕ and yields [13] $a_\pi/m_{\pi^0}^2 = 0.5(1 + m_\rho^2/m_\omega^2)/m_\rho^2 \approx 1.648\ \mathrm{GeV}^{-2}$ (or $a_\pi \approx 0.0300$) for the π^0 Dalitz decay. A more modern VMD prediction, which also includes the ϕ-meson contribution, leads to $a_\pi \approx 0.0305$ [16].

Another feature of this decay amplitude is an angular anisotropy of the virtual photon decaying into the e^+e^- pair, which also determines the density of events along $m^2(\gamma e^{+/-})$ of the $\pi^0 \to e^+e^-\gamma$ Dalitz plot. For the e^+, e^-, and γ in the π^0 rest frame, the angle θ^* between the direction of one of the leptons in the virtual-photon (or the dilepton) rest frame and the direction of the dilepton system (which is opposite to the γ direction) follows the dependence [17]

$$f(\cos\theta^*) = 1 + \cos^2\theta^* + \left(\frac{2m_e}{m_{ee}}\right)^2 \sin^2\theta^*, \quad (3)$$

with the $\sin^2\theta^*$ term becoming very small when $m_{ee} \gg 2m_e$.

Both the [QED(m_{ee})] term in Eq. (1) and the angular dependence in Eq. (3) represent only the leading-order term of the $\pi^0 \to e^+e^-\gamma$ decay amplitude, and radiative corrections need to be considered for a more accurate calculation of [QED($m_{ee}, \cos\theta^*$)]. The most recent calculations of radiative corrections to the differential decay rate of the Dalitz decay $\pi^0 \to e^+e^-\gamma$ were reported in Ref. [18]. In that paper, the results of the classical work of Mikaelian and Smith [19] were recalculated, and the missing one-photon irreducible contribution at the one-loop level was included. Typically radiative corrections make the angular dependence of the virtual-photon decay weaker. For the π^0 Dalitz decay, the corrected [QED] term integrated over $\cos\theta^*$ is ∼1% larger than the leading-order term at $q = 15$ MeV and becomes ∼10% lower at $q = 120$ MeV.

Despite the existence of recent high-statistics experiments searching for a dark-photon signal in $\pi^0 \to e^+e^-\gamma$ decays [10,11], the magnitude of the Dalitz-decay slope parameter a_π and its uncertainty in the Review of Particle Physics (RPP) [15], $a_\pi = 0.032 \pm 0.004$, are mostly determined by a measurement of the spacelike π^0 TFF in the process $e^+e^- \to e^+e^-\pi^0$ by the CELLO detector [20]. Extrapolating this spacelike TFF under the assumption of the validity of VMD, the value $a_\pi = 0.0326 \pm 0.0026_{\mathrm{stat}} \pm 0.0026_{\mathrm{syst}}$ has been extracted. It should be noted, however, that this result not only introduces a certain model dependence, but also requires an extrapolation from the range of momentum transfers ($q^2 > 0.5\ \mathrm{GeV}^2$), where the actual measurement took place, toward small q^2. Further improvement in measuring the spacelike π^0 TFF in the process $e^+e^- \to e^+e^-\pi^0$ is expected from the BESIII detector [21]. Because this measurement will cover smaller q^2, the precision in the slope parameter obtained by the extrapolation could be improved even more.

To check the consistency of the a_π values extracted from measurements at negative and positive q^2, the precision in the slope parameter obtained from measuring the Dalitz decays should be comparable with the results of extrapolating the spacelike TFFs. So far, the most accurate slope-parameter value obtained from measuring $\pi^0 \to e^+e^-\gamma$ decays, $a_\pi =$

$0.025 \pm 0.014_{\text{stat}} \pm 0.026_{\text{syst}}$ [22], has uncertainties one order of magnitude larger than the value from CELLO [20]. This timelike measurement is based on the analysis of just 54×10^3 $\pi^0 \to e^+e^-\gamma$ decays, with radiative corrections according to Ref. [19], and does not provide any $|F_{\pi^0\gamma}(m_{ee})|^2$ data points. The results of the present work are going to improve the experimental situation for the timelike π^0 TFF, with the experimental statistic of $\pi^0 \to e^+e^-\gamma$ decays larger by one order of magnitude, compared to Ref. [22]. Further improvement in the timelike region is expected to be made by the NA62 experiment, the preliminary result of which, $a_\pi = 0.0370 \pm 0.0053_{\text{stat}} \pm 0.0036_{\text{syst}}$, was based on 1.05×10^6 $\pi^0 \to e^+e^-\gamma$ decays observed [23]. The latest NA62 value for the slope parameter, which appeared after this paper was submitted for publication, updated their result to $a_\pi = 0.0368 \pm 0.0051_{\text{stat}} \pm 0.0025_{\text{syst}} = 0.0368 \pm 0.0057_{\text{tot}}$, based on 1.11×10^6 $\pi^0 \to e^+e^-\gamma$ decays observed [24].

Recent theoretical calculations for the $\pi^0 \to \gamma^*\gamma \to e^+e^-\gamma$ TFF, in addition to the slope parameter a_π, also involve the curvature parameter b_π:

$$F_{\pi^0\gamma}(m_{ee}) = 1 + a_\pi \frac{m_{ee}^2}{m_{\pi^0}^2} + b_\pi \frac{m_{ee}^4}{m_{\pi^0}^4}. \tag{4}$$

A calculation based on a model-independent method using Padé approximants was reported in Ref. [25]. The analysis of spacelike data (CELLO [20], CLEO [26], BABAR [27], and Belle [28]) with this method provides a good and systematic description of the low energy region, resulting in $a_\pi = 0.0324 \pm 0.0012_{\text{stat}} \pm 0.0019_{\text{syst}}$ and $b_\pi = (1.06 \pm 0.09_{\text{stat}} \pm 0.25_{\text{syst}}) \times 10^{-3}$. Values with even smaller uncertainties, $a_\pi = 0.0307 \pm 0.0006$ and $b_\pi = (1.10 \pm 0.02) \times 10^{-3}$, were recently obtained by using dispersion theory [16]. In that analysis, the singly virtual TFF was calculated in both the timelike and the spacelike regions, based on data for the $e^+e^- \to 3\pi$ cross section, generalizing previous studies on $\omega/\phi \to 3\pi$ decays [29] and $\gamma\pi \to \pi\pi$ scattering [30], and verifying the results by comparing them to timelike $e^+e^- \to \pi^0\gamma$ data at larger momentum transfer.

The capability of the A2 experimental setup to measure Dalitz decays was demonstrated in Refs. [31,32] for $\eta \to e^+e^-\gamma$. Measuring $\pi^0 \to e^+e^-\gamma$ is challenging because of the smallness of the TFF effect in the region of very low momentum transfer; the magnitude of $|F_{\pi^0\gamma}|^2$ is expected to reach only a 5% enhancement above the pure QED dependence at $m_{ee} = 120$ MeV/c^2. Thus, such a measurement requires high statistics to reach a statistical accuracy comparable with the expected TFF effect. Also, the magnitude of systematic uncertainties caused by the acceptance determination, background subtraction, and experimental resolutions needs to be small. The advantage of measuring $\pi^0 \to e^+e^-\gamma$ with the A2 setup at the Mainz Microtron (MAMI) is that π^0 mesons can be produced in the reaction $\gamma p \to \pi^0 p$, which has a very large cross section at energies close to the $\Delta(1232)$ state, and there is no background from other physical reactions at these energies. The only background for $\pi^0 \to e^+e^-\gamma$ decays are $\pi^0 \to \gamma\gamma$ decays with a photon converting into an e^+e^- pair in the material in front of electromagnetic calorimeters.

New results for the $\pi^0\gamma$ e/m TFF presented in this paper are based on an analysis of $\sim 4 \times 10^5 \pi^0 \to e^+e^-\gamma$ decays detected in the A2 experimental setup and using the radiative corrections from Ref. [18]. In addition to a value for the slope parameter a_π, the present TFF results include $|F_{\pi^0\gamma}(m_{ee})|^2$ data points with their total uncertainties, which allows a more fair comparison of the data with theoretical calculations or the use of the data in model-independent fits. Previously, the same A2 data sets were used for measuring π^0 photoproduction on the proton [33,34].

II. EXPERIMENTAL SETUP

The process $\gamma p \to \pi^0 p \to e^+e^-\gamma p$ was measured by using the Crystal Ball (CB) [35] as a central calorimeter and TAPS [36,37] as a forward calorimeter. These detectors were installed in the energy-tagged bremsstrahlung photon beam of the Mainz Microtron (MAMI) [38,39]. The photon energies were determined by using the Glasgow–Mainz tagging spectrometer [40–42].

The CB detector is a sphere consisting of 672 optically isolated NaI(Tl) crystals, shaped as truncated triangular pyramids, which point toward the center of the sphere. The crystals are arranged in two hemispheres that cover 93% of 4π, sitting outside a central spherical cavity with a radius of 25 cm, which holds the target and inner detectors. In this experiment, TAPS was arranged in a plane consisting of 384 BaF_2 counters of hexagonal cross section. It was installed 1.5 m downstream of the CB center and covered the full azimuthal range for polar angles from 1° to 20°. More details on the energy and angular resolution of the CB and TAPS are given in Refs. [43,44].

The present measurement used electron beams with energies 855 and 1557 MeV from the Mainz Microtron, MAMI-C [39]. The data with the 855-MeV beam were taken in 2008 (Run I) and those with the 1557-MeV beam in 2013 (Run II). Bremsstrahlung photons, produced by the beam electrons in a radiator (100-μm-thick diamond and 10-μm Cu for Run I and Run II, respectively) and collimated by a Pb collimator (with diameters 3 and 4 mm for Run I and Run II, respectively), were incident on a 10-cm-long liquid hydrogen (LH_2) target located in the center of the CB. The total amount of material around the LH_2 target, including the Kapton cell and the 1-mm-thick carbon-fiber beamline, was equivalent to 0.8% of a radiation length X_0. In the present measurement, it was essential to keep the material budget as low as possible to minimize the background from $\pi^0 \to \gamma\gamma$ decays with conversion of the photons into e^+e^- pairs.

The target was surrounded by a particle identification (PID) detector [46] used to distinguish between charged and neutral particles. It is made of 24 scintillator bars (50 cm long, 4 mm thick) arranged as a cylinder with a radius of 12 cm. A general sketch of the CB, TAPS, and PID is shown in Fig. 1. A multiwire proportional chamber, MWPC, also shown in this figure (which consists of two cylindrical MWPCs inside each other), was not used in the present measurements because of its relatively low efficiency for detecting $e^{+/-}$.

In Run I, the energies of the incident photons were analyzed from 140 up to 798 MeV by detecting the postbremsstrahlung electrons in the Glasgow tagged-photon spectrometer (Glas-

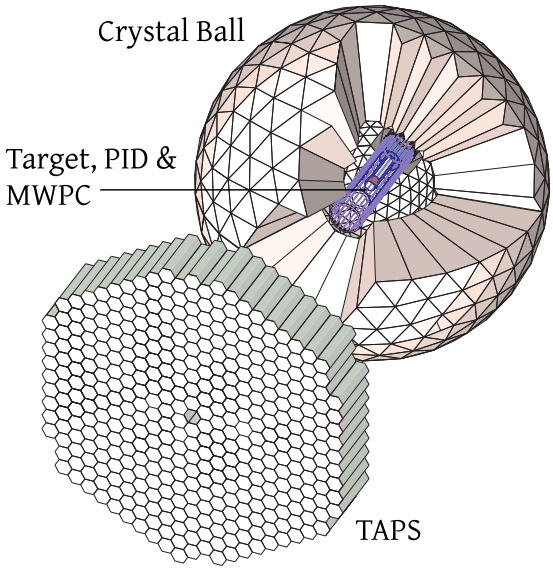

FIG. 1. A general sketch of the Crystal Ball, TAPS, and particle identification (PID) detectors.

gow tagger) [40–42], and from 216 up to 1448 MeV in Run II. The uncertainty in the energy of the tagged photons is mainly determined by the segmentation of tagger focal-plane detector in combination with the energy of the MAMI electron beam used in the experiments. Increasing the MAMI energy increases the energy range covered by the spectrometer and also has the corresponding effect on the uncertainty in E_γ. For the MAMI energy settings of 855 and 1557 MeV, this uncertainty was about ± 1 MeV and ± 2 MeV, respectively. More details on the tagger energy calibration and uncertainties in the energies can be found in Ref. [45].

The experimental trigger in Run I required the total energy deposited in the CB to exceed ∼100 MeV and the number of so-called hardware clusters in the CB (multiplicity trigger) to be two or more. In the trigger, a hardware cluster in the CB was a block of 16 adjacent crystals in which at least one crystal had an energy deposit larger than 30 MeV. In Run II, the trigger only required the total energy in the CB to exceed ∼120 MeV. More details on the experimental conditions of Run I and Run II can be found in Refs. [33,34].

III. DATA HANDLING

A. Event selection

To search for a signal from $\pi^0 \to e^+e^-\gamma$ decays, candidates for the process $\gamma p \to e^+e^-\gamma p$ were extracted from events having three or four clusters reconstructed by a software analysis in the CB and TAPS together. The offline cluster algorithm was optimized for finding a group of adjacent crystals in which the energy was deposited by a single-photon e/m shower. This algorithm works well for $e^{+/-}$, which also produce e/m showers in the CB and TAPS, and for proton clusters. The software threshold for the cluster energy was chosen to be 12 MeV. For the $\gamma p \to e^+e^-\gamma p$ candidates, the three-cluster events were analyzed assuming that the final-state proton was not detected. To diminish possible background from $\gamma p \to \pi^0\pi^0 p$ and $\gamma p \to \pi^0\pi^+ n$, the selected energy range was limited to $E_\gamma < 450$ MeV. To take the energies with the largest π^0 cross sections, $E_\gamma > 167$ MeV was required for Run I and $E_\gamma > 216$ MeV for Run II, in which the lower E_γ were not tagged. Note that a large fraction of π^0 events in this energy range are produced with the recoil proton below its detection threshold.

The selection of candidate events and the reconstruction of the reaction kinematics were based on the kinematic-fit technique. Details of the kinematic-fit parametrization of the detector information and resolutions are given in Ref. [43]. Because the three-cluster sample, in which there are good $\gamma p \to \pi^0 p \to e^+e^-\gamma p$ events without the outgoing proton detected, was mostly dominated by $\gamma p \to \pi^0 p \to \gamma\gamma p$ events, the latter kinematic-fit hypothesis was tested first. Then all events for which the confidence level (CL) to be $\gamma p \to \pi^0 p \to \gamma\gamma p$ was greater than 10^{-5} were discarded from further analysis. It was checked that such a preselection practically does not cause any losses of $\pi^0 \to e^+e^-\gamma$ decays, but rejects a significant background from two-photon final states. Because e/m showers from electrons and positrons are very similar to those of photons, the hypothesis $\gamma p \to 3\gamma p$ was tested to identify the $\gamma p \to e^+e^-\gamma p$ candidates. The events that satisfied this hypothesis with the CL greater than 1% were accepted for further analysis. The kinematic-fit output was used to reconstruct the kinematics of the outgoing particles. In this output, there was no separation between e/m showers caused by the outgoing photon, electron, or positron. Because the main purpose of the experiments was to measure the $\pi^0 \to e^+e^-\gamma$ decay rate as a function of the invariant mass $m(e^+e^-)$, the next step in the analysis was the separation of e^+e^- pairs from final-state photons. This procedure was optimized by using a Monte Carlo (MC) simulation of the signal events.

Because of the limited experimental resolution in the invariant mass $m(e^+e^-)$ (the average value of σ_m for which was ∼5.7 and ∼6.0 MeV for Run I and Run II, respectively) and the detection threshold for particles in the experimental setup, the MC simulation was made to be as similar as possible to the real $\gamma p \to \pi^0 p \to e^+e^-\gamma p$ events. This condition was important to minimize systematic uncertainties in the determination of experimental acceptances and to measure the TFF energy dependence properly. To reproduce the experimental yield of π^0 mesons and their angular distributions as a function of the incident-photon energy, the $\gamma p \to \pi^0 p$ reaction was generated according to the numbers of the corresponding π^0 events and their angular distributions measured in the same experiments [33,34]. The $\pi^0 \to e^+e^-\gamma$ decays were generated according to Eq. (1), with the phase-space term removed and assuming the RPP value, $a_\pi = 0.032$ [15], for the TFF dependence. The angular dependence of the virtual photon decaying into the e^+e^- pair was generated according to Eq. (3). Then these dependencies from the leading-order QED term of the decay amplitude were convoluted with radiative corrections based on the calculations of Ref. [18]. The event vertices were generated uniformly along the 10-cm-long LH_2 target.

The main background process, $\gamma p \to \pi^0 p \to \gamma\gamma p$, was also studied by using the MC simulation. The yield and the

production angular distributions of $\gamma p \to \pi^0 p$ were generated in the same way as for the process $\gamma p \to \pi^0 p \to e^+e^-\gamma p$.

For both π^0 decay modes, the generated events were propagated through a GEANT (version 3.21) simulation of the experimental setup. To reproduce the resolutions observed in the experimental data, the GEANT output (energy and timing) was subject to additional smearing, thus allowing both the simulated and experimental data to be analyzed in the same way. Matching the energy resolution between the experimental and MC events was achieved by adjusting the invariant-mass resolutions, the kinematic-fit stretch functions (or pulls), and probability distributions. Such an adjustment was based on the analysis of the same data sets for the reaction $\gamma p \to \pi^0 p \to \gamma\gamma p$, having almost no background from other physical reactions at these energies. The simulated events were also tested to check whether they passed the trigger requirements.

The PID detector was used to identify the final-state e^+e^- pair in the events initially selected as $\gamma p \to 3\gamma p$ candidates. Note that the detection efficiency for $e^{+/-}$ that pass through the PID is close to 100%. Because, with respect to the LH_2 target, the PID provides a full coverage merely for the CB crystals, only events with three e/m showers in the CB were selected for further analysis. This criterion also made all selected events pass the trigger requirements on both the total energy in the CB (Run I and Run II) and the multiplicity (Run I). The identification of $e^{+/-}$ in the CB was based on a correlation between the ϕ angles of fired PID elements with the angles of e/m showers in the calorimeter. The MC simulation of $\gamma p \to \pi^0 p \to e^+e^-\gamma p$ was used to optimize this procedure, minimizing the probability for misidentification of $e^{+/-}$ with the final-state photons. This procedure was optimized with respect to how close an e/m shower in the CB should be to a fired PID element to be considered as $e^{+/-}$ (namely $\Delta\phi < 18^\circ$), and how far it should be to be considered as a photon ($\Delta\phi > 20^\circ$). This optimization decreases the efficiency in selecting true events for which the ϕ angle of the electron or the positron is close to the photon ϕ angle.

The analysis of the MC simulation for the main background reaction $\gamma p \to \pi^0 p \to \gamma\gamma p$ revealed that this process could mimic $\pi^0 \to e^+e^-\gamma$ events when one of the final-state photons converted into an e^+e^- pair in the material between the production vertex and the NaI(Tl) surface. Because the opening angle between such electrons and positrons is typically very small, this background contributes mostly to low invariant masses $m(e^+e^-)$. A significant suppression of this background can be reached by requiring e^+ and e^- to be identified by different PID elements. However, such a requirement also decreases the detection efficiency for actual $\pi^0 \to e^+e^-\gamma$ events, especially at low invariant masses $m(e^+e^-)$. In further analysis of $\pi^0 \to e^+e^-\gamma$ events, both options, with larger and smaller background remaining from $\pi^0 \to \gamma\gamma$, were tested.

Another background source from $\gamma p \to \pi^0 p \to \gamma\gamma p$ are events that survived the CL $< 10^{-5}$ cut from testing this hypothesis itself. If one photon deposits some energy in the PID, then this e/m shower, together with the recoil proton, could be misidentified as an e^+e^- pair. Such background does not mimic the $\pi^0 \to e^+e^-\gamma$ peak, but the suppression of this background improves the signal-to-background ratio, which is important for more reliable fitting of the signal peak above the remaining background. Similar background can come from the $\gamma p \to \pi^0 p \to e^+e^-\gamma p$ events themselves when one of the leptons failed to be detected, and the recoil proton was misidentified with this lepton. The background from the misidentification of the recoil proton with $e^{+/-}$ can be suppressed by the analysis of energy losses, dE/dx, in the PID elements. To reflect the actual differential energy deposit dE/dx in the PID, the energy signal from each element, ascribed to either e^+ or e^-, was multiplied by the sine of the polar angle of the corresponding particle, the magnitude of which was taken from the kinematic-fit output. All PID elements were calibrated so that the $e^{+/-}$ peak position matched the corresponding peak in the MC simulation. To reproduce the actual energy resolution of the PID with the MC simulation, the GEANT output for PID energies was subject to additional smearing, allowing the $e^{+/-}$ selection with dE/dx cuts to be very similar for the experimental data and MC. The PID energy resolution in the MC simulations was adjusted to match the experimental dE/dx spectra for the $e^{+/-}$ particles from $\pi^0 \to e^+e^-\gamma$ decays observed experimentally. Possible systematic uncertainties due to the dE/dx cuts were checked via the stability of the results after narrowing the dE/dx range for selecting $e^{+/-}$.

The experimental dE/dx resolution of the PID for $e^{+/-}$ in Run I and the comparison of it with the MC simulation is illustrated in Fig. 2. Figures 2(a) and 2(b) show (for the experimental data and the MC simulation, respectively) two-dimensional plots of the $e^{+/-}$ dE/dx value of the PID versus the energy of the corresponding clusters in the CB. As seen, there is no dE/dx dependence of $e^{+/-}$ on their energy in the CB, and applying cuts just on a dE/dx value is sufficient for suppressing backgrounds caused by misidentifying protons as $e^{+/-}$. The comparison of the experimental $e^{+/-}$ dE/dx distributions with the MC simulation is depicted in Fig. 2(c). A small difference in the tails of the $e^{+/-}$ peak can mostly be explained by some background remaining in the experimental spectrum. This background includes events with misidentified recoil protons, photons converting before reaching the crystal surface, and also a small fraction from accidental hits in the PID. The dE/dx distribution from the recoil protons for the selected four-cluster events is shown in Fig. 2(c) by the red line, illustrating a quite small overlapping range of $e^{+/-}$ and the protons. Typical PID cuts, which were tested, varied from requiring $dE/dx < 3.7$ MeV to $dE/dx < 2.7$ MeV to suppress background events with misidentified protons, showing no systematic effects in the final results.

In addition to the background contributions discussed above, there are two more background sources. The first source comes from interactions of incident photons in the windows of the target cell. The subtraction of this background was based on the analysis of data samples that were taken with an empty target. The weight for the subtraction of the empty-target spectra was taken as a ratio of the photon-beam fluxes for the data samples with the full and the empty target. Another background was caused by random coincidences of the tagger counts with the experimental trigger; its subtraction was

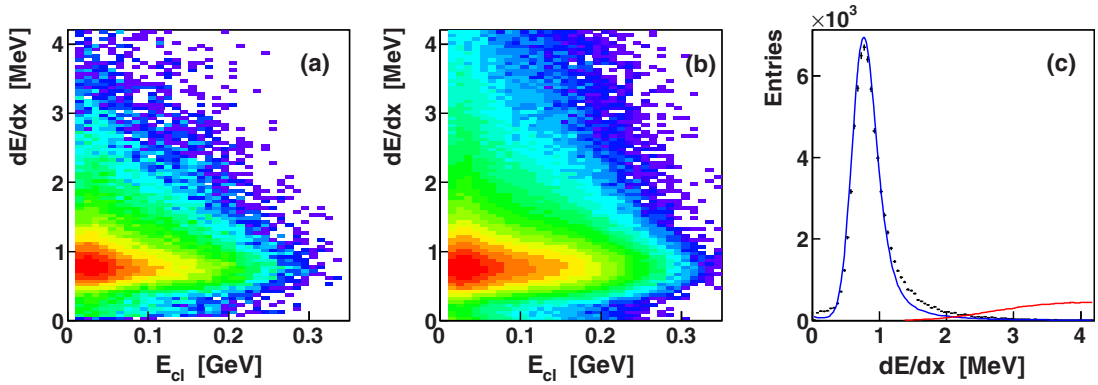

FIG. 2. Comparison of the $e^{+/-}$ dE/dx of the PID for experimental $\pi^0 \to e^+e^-\gamma$ decays and the MC simulation. The two-dimensional density distribution (with logarithmic scale along plot axis z) for the $e^{+/-}$ dE/dx of the PID versus the energy of the corresponding clusters in the CB is shown in (a) for the experimental data of Run I and in (b) for the MC simulation. The $e^{+/-}$ dE/dx distributions for the experimental data (crosses) and the MC simulation (blue solid line) are compared in (c). The dE/dx distribution from the recoil protons for the selected four-cluster events is shown in (c) by a red solid line.

carried out by using event samples for which all coincidences were random (see Refs. [43,44] for more details).

B. Analysis of $\pi^0 \to e^+e^-\gamma$ decays

To measure the $\pi^0 \to e^+e^-\gamma$ yield as a function of the invariant mass $m(e^+e^-)$, the selected candidate events were divided into several $m(e^+e^-)$ bins. Events with $m(e^+e^-) <$ 15 MeV/c^2 were not analyzed at all, because e/m showers from those e^+ and e^- start to overlap too much in the CB. The number of $\pi^0 \to e^+e^-\gamma$ decays in every $m(e^+e^-)$ bin was determined by fitting the experimental $m(e^+e^-\gamma)$ spectra with the π^0 peak rising above a smooth background.

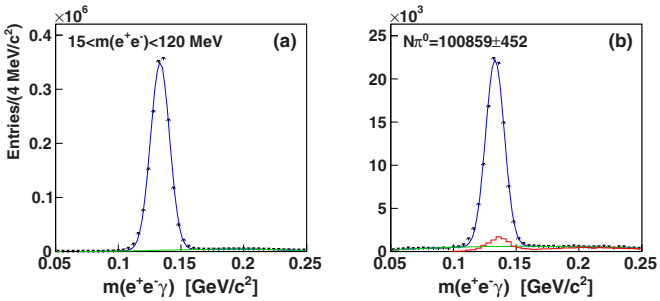

FIG. 3. $m(e^+e^-\gamma)$ invariant-mass distributions obtained in the analysis of Run I for the $m(e^+e^-)$ range from 15 to 120 MeV/c^2 with $\gamma p \to e^+e^-\gamma p$ candidates selected with the kinematic-fit CL $> 1\%$, a dE/dx PID cut accepting the entire range with deposits from $e^{+/-}$, and allowing both e^+ and e^- to be identified with the same PID element: (a) MC simulation of $\gamma p \to \pi^0 p \to e^+e^-\gamma p$ (black dots) fitted with the sum of a Gaussian (blue line) for the actual $\pi^0 \to e^+e^-\gamma$ peak and a polynomial (green line) of order 4 for the background from misidentifying the recoil proton as either e^+ or e^-; (b) experimental spectrum (black dots) after subtracting the background remaining from $\gamma p \to \pi^0 p \to \gamma\gamma p$. The $\pi^0 \to \gamma\gamma$ background, which is shown by a red line, is normalized to the number of subtracted events. The experimental distribution is fitted with the sum of a Gaussian (blue line) for the $\pi^0 \to e^+e^-\gamma$ peak and a polynomial (green line) of order 4 for the background.

The fitting procedure for $\pi^0 \to e^+e^-\gamma$ and the impact of selection criteria on the background is illustrated in Figs. 3–5. Figure 3 shows all $\gamma p \to e^+e^-\gamma p$ candidates from Run I in the $m(e^+e^-)$ range from 15 to 120 MeV/c^2, which were selected with the kinematic-fit CL $> 1\%$, a dE/dx PID cut accepting the entire range with deposits from $e^{+/-}$, and also allowing both e^+ and e^- to be identified with the same PID element. Figure 3(a) depicts the $m(e^+e^-\gamma)$ invariant-mass distribution for the MC simulation of $\gamma p \to \pi^0 p \to e^+e^-\gamma p$ fitted with the sum of a Gaussian for the actual $\pi^0 \to e^+e^-\gamma$ peak and a polynomial of order 4 for the background due to misidentifying the recoil proton as either e^+ or e^-. As shown, the background is very small, especially after the dE/dx PID cut. The experimental distribution after subtracting the random and empty-target backgrounds and the background remaining from $\gamma p \to \pi^0 p \to \gamma\gamma p$ is shown by black points in Fig. 3(b). The distribution for the $\pi^0 \to \gamma\gamma$ background is normalized to the number of subtracted events and is shown in the same figure by a red solid line. The subtraction normalization was based on the number of events generated for $\gamma p \to \pi^0 p \to \gamma\gamma p$ and the number of $\gamma p \to \pi^0 p$ events produced in the experiment. The experimental distribution was fitted with the sum of a Gaussian for the $\pi^0 \to e^+e^-\gamma$ peak and a polynomial of order 4 for the background. The centroid and width of the Gaussian obtained in both the fits (to the MC-simulation spectra and to the experimental spectra) are in good agreement with

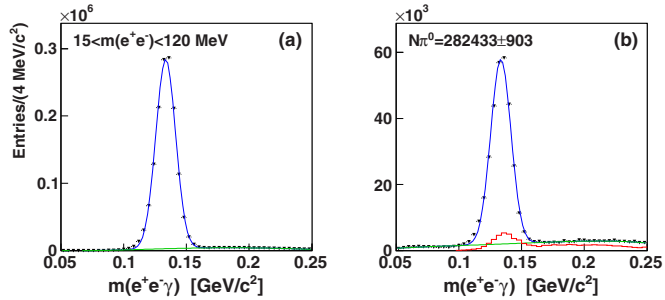

FIG. 4. Same as Fig. 3, but for Run II.

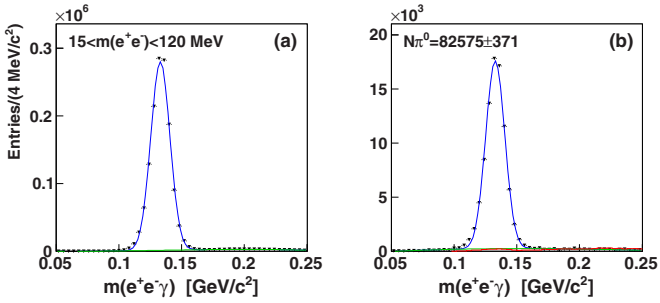

FIG. 5. Same as Fig. 3, but requiring both e^+ and e^- to be identified by different PID elements.

each other. This confirms the agreement of the experimental data and the MC simulation in the energy calibration of the calorimeters and their resolution. The order of the polynomial was chosen to be sufficient for a reasonable description of the background distribution in the range of fitting.

The number of $\pi^0 \to e^+e^-\gamma$ decays in both the MC-simulation and the experimental $m(e^+e^-\gamma)$ spectra was determined from the area under the Gaussian. For the selection criteria and the $m(e^+e^-)$ range used to obtain the spectra in Fig. 3, the averaged detection efficiency was determined to be 23.2%.

Figure 4 depicts the $\pi^0 \to e^+e^-\gamma$ sample obtained from Run II. The selection criteria here were identical to the cuts used to plot Fig. 3. As shown, the experimental statistic of Run II is almost three times larger, compared to Run I. However, the PID energy resolution was poorer in Run II, allowing slightly more background under the $\pi^0 \to e^+e^-\gamma$ peak and resulting in a slightly lower detection efficiency.

Using events of Run I, Fig. 5 illustrates the effect of requiring both e^+ and e^- to be identified by different PID elements. As seen, compared to Fig. 3(b), the level of background contributions, including $\pi^0 \to \gamma\gamma$, under the $\pi^0 \to e^+e^-\gamma$ peak becomes very small, whereas the average detection efficiency decreases to 18.7%. The results for the $\pi^0 \to e^+e^-\gamma$ yield, obtained with and without adding events with e^+ and e^- identified by the same PID element, showed good agreement within the fit uncertainties, confirming the reliability in the subtraction of the remaining $\pi^0 \to \gamma\gamma$ background.

The requirement that both e^+ and e^- be identified by different PID elements results in almost full elimination of the background contributions under the $\pi^0 \to e^+e^-\gamma$ peak. This enables measurement of the $\pi^0 \to \gamma\gamma^* \to \gamma e^+e^-$ angular dependence of the virtual photon decaying into an e^+e^- pair and comparison with Eq. (3). The experimental results for such an angular dependence are illustrated in Fig. 6 for events from the $\pi^0 \to e^+e^-\gamma$ peak of Run I. Figure 6(a) shows the experimental $\cos\theta^*$ distribution. The angular acceptance determined from the MC simulation is depicted in Fig. 6(b). The experimental distribution corrected for the acceptance is depicted in Fig. 6(c) and shows good agreement with the expected $1 + \cos^2\theta^*$ dependence. The deviation from this dependence due to radiative corrections is just few percent at the extreme angles. Because e^+ and e^- cannot be separated in the present experiment, the angles of both leptons were used to measure the dilepton decay dependence, which resulted in a symmetric shape with respect to $\cos\theta^* = 0$.

The statistics available for Run I and Run II and the level of background for $\pi^0 \to e^+e^-\gamma$ decays enabled division of all candidate events into 18 bins, covering the $m(e^+e^-)$ range from 15 to 120 MeV/c^2. The bins are 5 MeV wide up to 90 MeV/c^2, and 10 MeV wide at higher masses. Fits to the spectra were made separately for Run I and Run II, and the final results were combined together as independent measurements. The fitting procedure was the same as shown in Figs. 3–5.

IV. RESULTS AND DISCUSSION

The total number of $\pi^0 \to e^+e^-\gamma$ decays initially produced in each $m(e^+e^-)$ bin was obtained by correcting the number of decays observed in each bin with the corresponding detection efficiency. The results for $|F_{\pi^0\gamma}(m_{e^+e^-})|^2$ were obtained from those initial numbers of $\pi^0 \to e^+e^-\gamma$ decays by taking into account the total number of $\pi^0 \to \gamma\gamma$ decays produced in

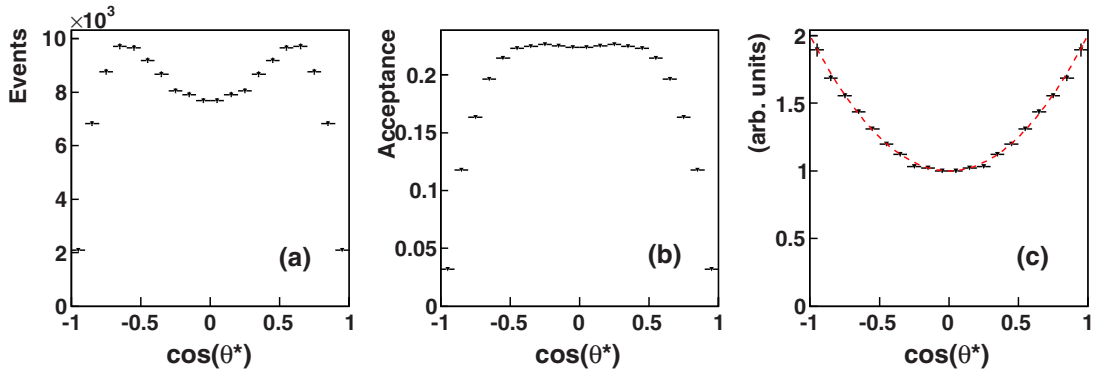

FIG. 6. The $\pi^0 \to \gamma\gamma^* \to \gamma e^+e^-$ angular dependence (in the π^0 rest frame) of the virtual photon decaying into a e^+e^- pair, with θ^* being the angle between the direction of one of the leptons in the virtual-photon (or the dilepton) rest frame and the direction of the dilepton system (which is opposite to the γ direction): (a) experimental events from the $\pi^0 \to \gamma e^+e^-$ peak; (b) angular acceptance based on the MC simulation; (c) the experimental spectrum corrected for the acceptance and normalized for comparing to the $1 + \cos^2\theta^*$ dependence (shown by a red dashed line). Because e^+ and e^- cannot be separated in the present experiment, the angles of both leptons were used, resulting in a symmetric shape with respect to $\cos\theta^* = 0$.

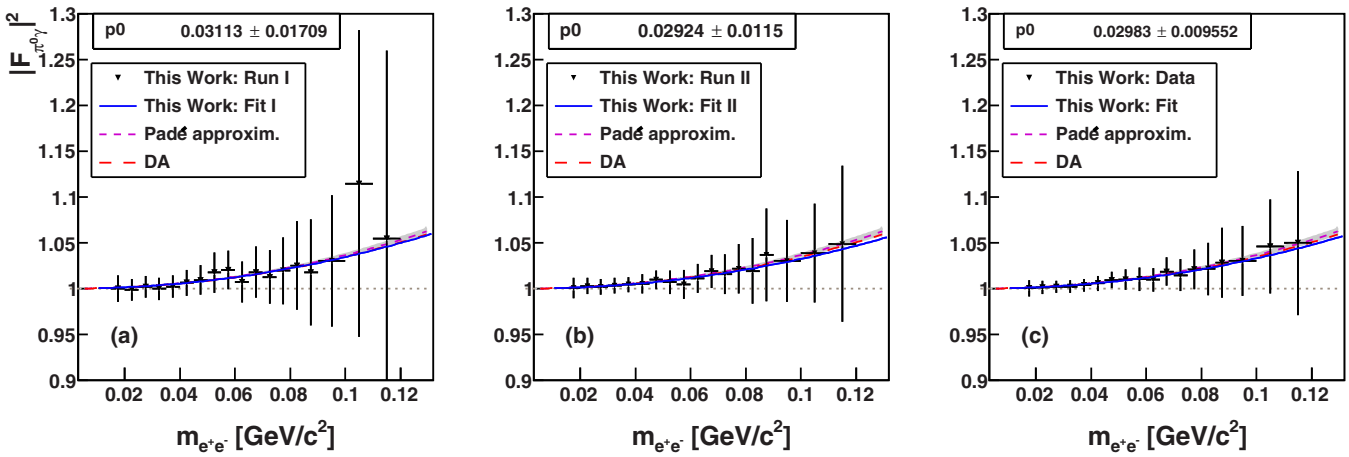

FIG. 7. $|F_{\pi^0\gamma}|^2$ results (black filled triangles) obtained from Run I (a), Run II (b), and the combined values (c) are fitted with Eq. (2) (shown by blue lines, with $p0$ being the slope parameter a_π) and compared to the calculations with Padé approximants [25] (shown by a short-dashed magenta line with an error band) and to the dispersive analysis (DA) from Ref. [16] (long-dashed red line). The error band for the latter analysis is narrower by a factor of 4, compared to the other shown, and was omitted because of its smallness. The error bars on all data points represent the total uncertainties of the results.

the same data sets [33,34] and the [QED(m_{ee})] term from Eq. (1) after radiative corrections according to the calculations of Ref. [18]. The uncertainty in an individual $|F_{\pi^0\gamma}(m_{e^+e^-})|^2$ value from a particular fit was based on the uncertainty in the number of decays determined by this fit (i.e, the uncertainty in the area under the Gaussian). The systematic uncertainties in the $|F_{\pi^0\gamma}(m_{e^+e^-})|^2$ values were estimated for each individual $m(e^+e^-)$ bin by repeating its fitting procedure several times after refilling the $m(e^+e^-\gamma)$ spectra with different combinations of selection criteria, which were used to improve the signal-to-background ratio, or after slight changes in the parametrization of the background under the signal peak. The changes in selection criteria included cuts on the kinematic-fit CL (such as 1% 2%, 5%, and 10%), different cuts on PID dE/dx, and switching on and off the requirement for both e^+ and e^- to be identified by different PID elements. The requirement of making several fits for each $m(e^+e^-)$ bin provided a check on the stability of the $|F_{\pi^0\gamma}(m_{e^+e^-})|^2$ results. The average of the results of all fits made for one bin was then used to obtain final TFF values that were more reliable than the results based on the fit with the largest number of $\pi^0 \to e^+e^-\gamma$ decays, corresponding to the initial selection criteria. Because the fits for a given $m(e^+e^-)$ bin with different selection criteria or different background parametrizations were based on the same initial data sample, the corresponding $|F_{\pi^0\gamma}(m_{e^+e^-})|^2$ results were correlated and could not be considered as independent measurements for calculating the uncertainty in the averaged TFF value. Thus, this uncertainty was taken from the fit with the largest number of $\pi^0 \to e^+e^-\gamma$ decays in the $m(e^+e^-)$ bin, which was a conservative estimate of the uncertainty in the averaged TFF value. The systematic uncertainty in the averaged $|F_{\pi^0\gamma}(m_{e^+e^-})|^2$ value was taken as the root mean square of the results from all fits made for this bin. The total uncertainty in this $|F_{\pi^0\gamma}(m_{e^+e^-})|^2$ value was calculated by adding in quadrature its fit (partially reflecting experimental statistics in the bin) and systematic uncertainties. In the end, the $|F_{\pi^0\gamma}(m_{e^+e^-})|^2$ results from Run I and Run II, which were independent measurements, were combined as a weighted average with weights taken as inverse values of their total uncertainties in quadrature.

The individual $|F_{\pi^0\gamma}(m_{e^+e^-})|^2$ results obtained from Run I, Run II, and their weighted average are depicted in Figs. 7(a)–7(c), respectively. The error bars plotted on all data points represent the total uncertainties of the results. Fits of the data points with Eq. (2) are shown by the blue solid lines. The fit parameter $p0$ corresponds to the slope parameter a_π. Because the fits are made to the data points with their total uncertainties, the fit errors for a_π give their total uncertainty as well. Fits that included a normalization parameter showed no need for such a parameter, so it was neglected in the end. The present experimental results depicted in Fig. 7 are also compared to the calculations with Padé approximants [25] and to the dispersive analysis (DA) from Ref. [16], which were discussed in the Introduction. As shown, all fits to the data points lie slightly lower than the calculations. However, the magnitude of the deviation is well within the experimental uncertainties. In addition, attempts to fit the present data points with Eq. (4) could not provide any reliable values for the curvature parameter b_π and resulted in a strong correlation between the parameters a_π and b_π. The comparison of the individual results obtained from Run I and Run II illustrates their good consistency within the error bars, even though the uncertainties from Run I are significantly larger than those from Run II.

Based on the fit to the data points combined from Run I and Run II, the magnitude obtained for the slope parameter,

$$a_\pi = 0.030 \pm 0.010_{\text{tot}}, \tag{5}$$

shows, within the uncertainties, good agreement with the RPP value, $a_\pi = 0.032 \pm 0.004$ [15], and with the calculations from Ref. [25], $a_\pi = 0.0324 \pm 0.0012_{\text{stat}} \pm 0.0019_{\text{syst}}$, and Ref. [16], $a_\pi = 0.0307 \pm 0.0006$. Though the uncertainty obtained for a_π in the present measurement is significantly larger than in Refs. [15,16,25], the present result significantly

TABLE I. Results of this work for the π^0 TFF, $|F_{\pi^0\gamma}|^2$, as a function of the invariant mass $m(e^+e^-)$, listed for Run I, Run II, and their average, where the two uncertainties listed for Run I and Run II are fit (reflecting statistics) and systematic, respectively, and the total uncertainty is listed for the average.

$m(e^+e^-)$ (MeV/c^2)	17.5 ± 2.5	22.5 ± 2.5	27.5 ± 2.5	32.5 ± 2.5
Run I	$1.0001 \pm 0.0140 \pm 0.0035$	$0.9987 \pm 0.0114 \pm 0.0033$	$1.0018 \pm 0.0110 \pm 0.0044$	$0.9996 \pm 0.0110 \pm 0.0050$
Run II	$1.0003 \pm 0.0105 \pm 0.0036$	$1.0027 \pm 0.0085 \pm 0.0026$	$1.0019 \pm 0.0078 \pm 0.0032$	$1.0034 \pm 0.0083 \pm 0.0020$
Run I + Run II	1.0002 ± 0.0088	1.0013 ± 0.0071	1.0018 ± 0.0069	1.0021 ± 0.0070
$m(e^+e^-)$ (MeV/c^2)	37.5 ± 2.5	42.5 ± 2.5	47.5 ± 2.5	52.5 ± 2.5
Run I	$1.0022 \pm 0.0119 \pm 0.0034$	$1.0063 \pm 0.0132 \pm 0.0046$	$1.0093 \pm 0.0152 \pm 0.0053$	$1.0175 \pm 0.0165 \pm 0.0148$
Run II	$1.0044 \pm 0.0080 \pm 0.0022$	$1.0053 \pm 0.0098 \pm 0.0034$	$1.0095 \pm 0.0097 \pm 0.0040$	$1.0069 \pm 0.0125 \pm 0.0035$
Run I + Run II	1.0037 ± 0.0069	1.0057 ± 0.0084	1.0094 ± 0.0088	1.0096 ± 0.0112
$m(e^+e^-)$ (MeV/c^2)	57.5 ± 2.5	62.5 ± 2.5	67.5 ± 2.5	72.5 ± 2.5
Run I	$1.0203 \pm 0.0200 \pm 0.0068$	$1.0073 \pm 0.0207 \pm 0.0086$	$1.0179 \pm 0.0282 \pm 0.0021$	$1.0126 \pm 0.0289 \pm 0.0042$
Run II	$1.0046 \pm 0.0124 \pm 0.0098$	$1.0109 \pm 0.0141 \pm 0.0069$	$1.0188 \pm 0.0169 \pm 0.0068$	$1.0154 \pm 0.0205 \pm 0.0071$
Run I + Run II	1.0102 ± 0.0126	1.0097 ± 0.0129	1.0185 ± 0.0153	1.0144 ± 0.0174
$m(e^+e^-)$ (MeV/c^2)	77.5 ± 2.5	82.5 ± 2.5	87.5 ± 2.5	95.0 ± 5.0
Run I	$1.0194 \pm 0.0358 \pm 0.0065$	$1.0251 \pm 0.0480 \pm 0.0066$	$1.0178 \pm 0.0576 \pm 0.0076$	$1.0301 \pm 0.0694 \pm 0.0184$
Run II	$1.0214 \pm 0.0251 \pm 0.0100$	$1.0192 \pm 0.0317 \pm 0.0165$	$1.0365 \pm 0.0478 \pm 0.0167$	$1.0303 \pm 0.0430 \pm 0.0124$
Run I + Run II	1.0207 ± 0.0217	1.0213 ± 0.0288	1.0284 ± 0.0382	1.0302 ± 0.0380
$m(e^+e^-)$ (MeV/c^2)	105.0 ± 5.0	115.0 ± 5.0		
Run I	$1.115 \pm 0.167 \pm 0.011$	$1.054 \pm 0.203 \pm 0.031$		
Run II	$1.039 \pm 0.053 \pm 0.007$	$1.049 \pm 0.083 \pm 0.019$		
Run I + Run II	1.046 ± 0.051	1.050 ± 0.079		

improves the precision in the slope parameter a_π measured in the timelike region directly from the $\pi^0 \to e^+e^-\gamma$ decay and is much closer to the precision of the slope parameter extracted from the spacelike data [20]. The latest result from NA62, $a_\pi = 0.0368 \pm 0.0057_{\text{tot}}$ [24], is somewhat greater than all mentioned values but is consistent with them within the uncertainties.

The numerical values for the individual $|F_{\pi^0\gamma}(m_{e^+e^-})|^2$ results from Run I and Run II and for their weighted average are listed in Table I. To illustrate the magnitude of each kind of uncertainty, the individual results from Run I and Run II are listed with both fit and systematic uncertainties. The combined results are given with their total uncertainties. As shown in Table I, the total uncertainties are dominated by the contribution from the fit uncertainties, reflecting statistics. Thus, a more precise measurement of the π^0 TFF at low momentum transfer with the Dalitz decay $\pi^0 \to e^+e^-\gamma$ needs a significant increase in experimental statistics. The π^0 TFF parameters extracted from such a precision measurement could then constrain calculations that estimate the pion-exchange term, $a_\mu^{\pi^0}$, to the HLbL scattering contribution to $(g-2)_\mu$.

V. SUMMARY AND CONCLUSIONS

The Dalitz decay $\pi^0 \to e^+e^-\gamma$ has been measured in the $\gamma p \to \pi^0 p$ reaction with the A2 tagged-photon facility at the Mainz Microtron, MAMI. The value obtained for the slope parameter of the π^0 e/m TFF, $a_\pi = 0.030 \pm 0.010_{\text{tot}}$, agrees within the uncertainties with existing measurements of this decay and with recent theoretical calculations. The uncertainty obtained in the value of a_π is lower than in previous results based on the $\pi^0 \to e^+e^-\gamma$ decay. The results of this work also include $|F_{\pi^0\gamma}(m_{ee})|^2$ data points with their total uncertainties, which allows a more fair comparison of the experimental data with theoretical calculations or the use of those data in model-independent fits. A much more precise measurement of the π^0 TFF at low momentum transfer with the Dalitz decay $\pi^0 \to e^+e^-\gamma$, which has already been planned by the A2 Collaboration, hopefully will reach the accuracy needed to constrain calculations that estimate the pion-exchange term, $a_\mu^{\pi^0}$, to the HLbL scattering contribution to $(g-2)_\mu$.

ACKNOWLEDGMENTS

The authors wish to acknowledge the excellent support of the accelerator group and operators of MAMI. We would like to thank Bastian Kubis, Stefan Leupold, and Pere Masjuan for useful discussions and continuous interest in the paper. This work was supported by the Deutsche Forschungsgemeinschaft (SFB443, SFB/TR16, and SFB1044), DFG-RFBR (Grant No. 09-02-91330), the European Community-Research Infrastructure Activity under the FP6 "Structuring the European Research Area" program (Hadron Physics, Contract No. RII3-CT-2004-506078), Schweizerischer Nationalfonds (Contracts No. 200020-156983, No. 132799, No. 121781, No. 117601, and No. 113511), the U.K. Science and Technology Facilities Council (STFC 57071/1, 50727/1), the U.S. Department of Energy (Offices of Science and Nuclear Physics, Awards No. DE-FG02-99-ER41110, No. DE-FG02-88ER40415, and No. DE-FG02-01-ER41194) and National Science Foundation (Grants No. PHY-1039130 and No. IIA-1358175), NSERC of Canada (Grants No. 371543-2012 and No. SAPPJ-2015-00023), and INFN (Italy). We thank the undergraduate students of Mount Allison University and The George Washington University for their assistance.

[1] Proceedings of the First MesonNet Workshop on Meson Transition Form Factors, 2012, Cracow, Poland, edited by E. Czerwinski, S. Eidelman, C. Hanhart, B. Kubis, A. Kupść, S. Leupold, P. Moskal, and S. Schadmand, arXiv:1207.6556.
[2] T. Husek and S. Leupold, Eur. Phys. J. C **75**, 586 (2015).
[3] P. Masjuan and P. Sanchez-Puertas, J. High Energy Phys. 08 (2016) 108.
[4] G. Colangelo, M. Hoferichter, B. Kubis, M. Procura, and P. Stoffer, Phys. Lett. B **738**, 6 (2014).
[5] G. Colangelo, M. Hoferichter, M. Procura, and P. Stoffer, J. High Energy Phys. 09 (2015) 074.
[6] F. Jegerlehner and A. Nyffeler, Phys. Rep. **477**, 1 (2009).
[7] A. Nyffeler, Phys. Rev. D **94**, 053006 (2016).
[8] V. Pauk and M. Vanderhaeghen, Phys. Rev. D **90**, 113012 (2014).
[9] B. Batell, M. Pospelov, and A. Ritz, Phys. Rev. D **80**, 095024 (2009).
[10] J. R. Batley *et al.*, Phys. Lett. B **746**, 178 (2015).
[11] P. Adlarson *et al.*, Phys. Lett. B **726**, 187 (2013).
[12] N. M. Kroll and W. Wada, Phys. Rev. **98**, 1355 (1955).
[13] L. G. Landsberg, Phys. Rep. **128**, 301 (1985).
[14] J. J. Sakurai, *Currents and Mesons* (University of Chicago Press, Chicago, 1969).
[15] K. A. Olive *et al.* (Particle Data Group), Chin. Phys. C **38**, 090001 (2014).
[16] M. Hoferichter, B. Kubis, S. Leupold, F. Niecknig, and S. P. Schneider, Eur. Phys. J. C **74**, 3180 (2014).
[17] R. Arnaldi *et al.*, Phys. Lett. B **757**, 47 (2016).
[18] T. Husek, K. Kampf, and J. Novotný, Phys. Rev. D **92**, 054027 (2015).
[19] K. Mikaelian and J. Smith, Phys. Rev. D **5**, 1763 (1972).
[20] H. J. Behrend *et al.*, Z. Phys. C **49**, 401 (1991).
[21] C. F. Redmer (private communication).
[22] R. Meijer Drees *et al.*, Phys. Rev. D **45**, 1439 (1992).
[23] E. Goudzovski (for the NA48/2 and NA62 Collaborations), EPJ Web Conf. **130**, 01019 (2016); arXiv:1611.04972.
[24] C. Lazzeroni *et al.*, arXiv:1612.08162.
[25] P. Masjuan, Phys. Rev. D **86**, 094021 (2012).
[26] J. Gronberg *et al.*, Phys. Rev. D **57**, 33 (1998).
[27] P. del Amo Sanchez *et al.*, Phys. Rev. D **84**, 052001 (2011).
[28] S. Uehara *et al.*, Phys. Rev. D **86**, 092007 (2012).
[29] F. Niecknig, B. Kubis, and S. P. Schneider, Eur. Phys. J. C **72**, 2014 (2012)
[30] M. Hoferichter, B. Kubis, and D. Sakkas, Phys. Rev. D **86**, 116009 (2012).
[31] P. Aguar-Bartolome *et al.*, Phys. Rev. C **89**, 044608 (2014).
[32] H. Berghäuser *et al.*, Phys. Lett. B **701**, 562 (2011).
[33] D. Hornidge *et al.*, Phys. Rev. Lett. **111**, 062004 (2013).
[34] P. Adlarson *et al.*, Phys. Rev. C **92**, 024617 (2015).
[35] A. Starostin *et al.*, Phys. Rev. C **64**, 055205 (2001).
[36] R. Novotny, IEEE Trans. Nucl. Sci. **38**, 379 (1991).
[37] A. R. Gabler *et al.*, Nucl. Instrum. Methods Phys. Res. A **346**, 168 (1994).
[38] H. Herminghaus *et al.*, IEEE Trans. Nucl. Sci. **30**, 3274 (1983).
[39] K.-H. Kaiser *et al.*, Nucl. Instrum. Methods Phys. Res. A **593**, 159 (2008).
[40] I. Anthony *et al.*, Nucl. Instrum. Methods Phys. Res. A **301**, 230 (1991).
[41] S. J. Hall *et al.*, Nucl. Instrum. Methods Phys. Res. A **368**, 698 (1996).
[42] J. C. McGeorge *et al.*, Eur. Phys. J. A **37**, 129 (2008).
[43] S. Prakhov *et al.*, Phys. Rev. C **79**, 035204 (2009).
[44] E. F. McNicoll *et al.*, Phys. Rev. C **82**, 035208 (2010).
[45] A. Nikolaev *et al.*, Eur. Phys. J. A **50**, 58 (2014).
[46] D. Watts, *Proceedings of the 11th International Conference on Calorimetry in Particle Physics*, Perugia, Italy, 2004 (World Scientific, Singapore, 2005), p. 560.